
Functional Imaging Signature of Patients Presenting with Polycythemia/Paraganglioma Syndromes

Ingo Janssen^{1,2}, Clara C. Chen³, Zhenping Zhuang⁴, Corina M. Millo⁵, Katherine I. Wolf¹, Alexander Ling⁶, Frank I. Lin⁷, Karen T. Adams¹, Peter Herscovitch⁵, Richard A. Feelders⁸, Antonio T. Fojo⁹, David Taieb¹⁰, Electron Kebebew¹¹, and Karel Pacak¹

¹Section on Medical Neuroendocrinology, Eunice Kennedy Shriver National Institute of Child Health and Human Development, National Institutes of Health, Bethesda, Maryland; ²Department of Radiology and Nuclear Medicine, Section of Nuclear Medicine, University Hospital Schleswig Holstein, Lübeck, Germany; ³Nuclear Medicine Division, Radiology & Imaging Sciences, National Institutes of Health, Bethesda, Maryland; ⁴Surgical Neurology Branch, National Institute of Neurological Disorders and Stroke, National Institutes of Health, Bethesda, Maryland; ⁵Positron Emission Tomography Department, National Institutes of Health, Bethesda, Maryland; ⁶Radiology and Imaging Sciences, National Institutes of Health Clinical Center, Bethesda, Maryland; ⁷Cancer Imaging Program, National Cancer Institute, National Institutes of Health, Bethesda, Maryland; ⁸Division of Endocrinology, Department of Internal Medicine, Erasmus Medical Center, Rotterdam, The Netherlands; ⁹Endocrine Oncology Branch, National Cancer Institute, Bethesda, Maryland; ¹⁰Department of Nuclear Medicine, La Timone University Hospital, CERIMED, Aix-Marseille University, Marseille, France; and ¹¹Center for Cancer Research, National Cancer Institute, Bethesda, Maryland

Pheochromocytoma/paraganglioma (PPGL) syndromes associated with polycythemia have previously been described in association with mutations in the von Hippel–Lindau gene. Recently, mutations in the prolyl hydroxylase gene (*PHD*) 1 and 2 and in the hypoxia-inducible factor 2 α (*HIF2A*) were also found to be associated with multiple and recurrent PPGL. Such patients also presented with PPGL and polycythemia, and later on, some presented with duodenal somatostatinoma. In additional patients presenting with PPGL and polycythemia, no further mutations have been discovered. Because the functional imaging signature of patients with PPGL–polycythemia syndromes is still unknown, and because these tumors (in most patients) are multiple, recurrent, and metastatic, the goal of our study was to assess the optimal imaging approach using 4 different PET radiopharmaceuticals and CT/MRI in these patients. **Methods:** Fourteen patients (10 women, 4 men) with confirmed PPGL and polycythemia prospectively underwent ⁶⁸Ga-DOTATATE (13 patients), ¹⁸F-FDG (13 patients), ¹⁸F-fluorodihydroxyphenylalanine (¹⁸F-FDOPA) (14 patients), ¹⁸F-fluorodopamine (¹⁸F-FDA) (11 patients), and CT/MRI (14 patients). Detection rates of PPGL lesions were compared between all imaging studies and stratified between the underlying mutations. **Results:** ¹⁸F-FDOPA and ¹⁸F-FDA PET/CT showed similar combined lesion-based detection rates of 98.7% (95% confidence interval [CI], 92.7%–99.8%) and 98.3% (95% CI, 90.9%–99.7%), respectively. The detection rates for ⁶⁸Ga-DOTATATE (35.3%; 95% CI, 25.0%–47.2%), ¹⁸F-FDG (42.3; 95% CI, 29.9%–55.8%), and CT/MRI (60.3%; 95% CI, 48.8%–70.7%) were significantly lower ($P < 0.01$), irrespective of the mutation status. **Conclusion:** ¹⁸F-FDOPA and ¹⁸F-FDA are superior to ¹⁸F-FDG, ⁶⁸Ga-DOTATATE, and CT/MRI and should be the radiopharmaceuticals of choice in this rare group of patients.

Key Words: ¹⁸F-FDOPA; ¹⁸F-FDA; pheochromocytoma; paraganglioma; polycythemia

J Nucl Med 2017; 58:1236–1242

DOI: 10.2967/jnumed.116.187690

Pheochromocytomas/paragangliomas (PPGLs) are rare tumors derived from sympathetic tissue in adrenal or extraadrenal abdominal locations or from parasympathetic tissue in the thorax or head and neck (1). More than 35% of PPGLs are hereditary, including multiple endocrine neoplasia 2 and neurofibromatosis 1. In recent years, mutations in genes encoding the 4 subunits of the succinate dehydrogenase (*SDH*) complex (2–5), fumarate hydratase (6), and MYC-associated factor X (7) were identified and found to be associated with the presence of multiple and metastatic PPGLs.

In the last few years, hypoxia-inducible factors (HIFs) have been under thorough investigation and HIF 2 α (*HIF2A* also called *EPAS 1*) (8,9) as well as prolyl hydroxylase (*PHD*) 1 and *PHD2* mutations have been discovered (10,11) in patients with PPGLs. HIF also functions as a regulator of erythropoietin (12), and patients with mutations in these genes present with multiple, recurrent, and often metastatic PPGLs as well as with polycythemia at birth or in early childhood. A mutation in the von Hippel–Lindau (*VHL*) gene was previously known to lead to polycythemia via alteration in HIF protein stabilization (9). Patients without *HIF2A*, *PHD1*, or *PHD2* mutations, but with identical clinical presentations, have been evaluated at our institution. However, in these patients, no known mutations have been identified thus far. Nevertheless, they are strongly suggestive for carrying a yet to be discovered mutation that will lead to an alteration in the HIF signaling pathway, causing multiple PPGLs associated with polycythemia and elevated erythropoietin levels.

The functional imaging signature for patients with these PPGL–polycythemia syndromes has never been evaluated and is, therefore, currently unknown. However, these patients tend to present

Received Nov. 23, 2016; revision accepted Feb. 10, 2017.
For correspondence or reprints contact: Karel Pacak, National Institute of Child Health and Human Development, National Institutes of Health, Building 10, CRC, Rm. 1E-3140, 10 Center Dr. MSC-1109, Bethesda, MD 20892.
E-mail: karel@mail.nih.gov
Published online Mar. 23, 2017.
COPYRIGHT © 2017 by the Society of Nuclear Medicine and Molecular Imaging.

with recurrent and multiple tumors (8,11), along with metastatic disease (11). Proper staging and early detection of multiple and recurrent lesions or metastatic disease is a critical clinical decision-making point for choosing an appropriate treatment, follow-up, and counseling plan. Therefore, our goal was to evaluate the optimal functional imaging approach in these patients by investigating the currently established and promising radiopharmaceuticals and stratifying these patients by mutation status (*HIF2A*, *PHD*, and unknown mutations). We evaluated ^{68}Ga -DOTATATE, ^{18}F -FDG, ^{18}F -fluorodihydroxyphenylalanine (^{18}F -FDOPA), and ^{18}F -fluorodopaamine (^{18}F -FDA). All patients underwent anatomic imaging with whole-body CT/MRI.

When available, histopathologic proof served as our gold standard. When histologic proof was neither feasible nor ethical for lesion detection, the composite of both anatomic and all functional imaging tests was considered the imaging comparator, as previously described and supported (13,14).

MATERIALS AND METHODS

Between February 2014 and November 2015, 14 consecutive patients (4 men, 10 women) with PPGL–polycythemia syndromes with a mean age of 37.0 ± 14.7 y were prospectively evaluated at the Eunice Kennedy Shriver National Institute of Child Health and Human Development (NICHD) at the National Institutes of Health (NIH). All patients had proven PPGLs based on histopathology as well as a history of polycythemia requiring phlebotomy. Most patients continued with follow-up in 2016.

The study protocol was approved by the institutional review board of the Eunice Kennedy Shriver NICHD (NCT00004847). All patients provided written informed consent for all clinical, genetic, biochemical, and imaging studies regarding PPGLs.

The mean age at diagnosis of primary PPGLs in these patients was 27.6 ± 13.1 y. All 14 patients previously underwent resection of their primary PPGLs, some of them requiring multiple

operations. Individual patient characteristics are summarized in Tables 1 and 2.

Imaging Techniques

All CT and MRI scans of the neck, chest, abdomen, and pelvis were obtained as follows and previously described (13). CT scans of the neck, chest, abdomen, and pelvis were obtained using the following devices: Somatom Definition AS and Somatom Definition Flash (Siemens Medical Solutions) and Aquilion ONE (Toshiba Medical Systems). Section thickness was up to 3 mm in the neck and 5 mm through the chest, abdomen, and pelvis. All studies were performed with intravenous rapid infusion of nonionic water-soluble contrast agent as well as oral contrast material.

MRI scans of the neck, chest, abdomen, and pelvis were obtained with 1.5- and 3-T scanners (Achieva 1.5 and 3 T [Philips]; Verio 1.5-T [Siemens Medical Solutions]). Image thickness was 5 mm for all neck studies and 6 mm for chest, abdominal, and pelvic scans. Pre- and postinjection images were obtained in the axial plane. All MRI scans included axial T2 series with and without fat saturation, short tau inversion recovery series, and T1 pre- and postcontrast series. MRI scans of the abdomen and pelvis also included axial T1 in and out of phase and dynamic T1-weighted high-resolution isotropic volume examination during infusion of contrast, followed by delayed axial and coronal postcontrast scans after intravenous injection of a gadolinium–diethylenetriamine pentaacetic acid contrast agent.

Seven patients underwent both CT and MRI studies, whereas the remaining 7 underwent MRI scans only. All 14 patients underwent ^{18}F -FDOPA PET/CT scanning, with 13 patients also undergoing ^{68}Ga -DOTATATE, 12 ^{18}F -FDG, and 11 ^{18}F -FDA PET/CT scanning.

PET/CT scans from the upper thighs to the skull were acquired 60 min after intravenous injection of a mean administered activity of 185.7 ± 21.4 MBq of ^{68}Ga -DOTATATE, 60 min after 284.7 ± 74.8 MBq of ^{18}F -FDG, 30 min after 420.5 ± 110.2 MBq of ^{18}F -FDOPA, and approximately 8 min after 39.3 ± 0.7 MBq of ^{18}F -FDA. Sixty minutes before each ^{18}F -FDOPA scan, 200 mg of carbidopa was administered orally. All PET/CT scans were acquired on Biograph-mCT 64 and Biograph-mCT 128 PET/CT scanners (Siemens Medical

TABLE 1
Individual Patient Characteristics

Patient no.	Sex	Mutation	Age (d)	Age (s)	Location of primary tumor	Hypersecretion
1	F	<i>HIF2A</i>	38	40	R perirenal	NE, MTT, CgA
2	F	<i>HIF2A</i>	18	24	R adrenal	DA, MTT
3	F	<i>HIF2A</i>	14	33	L paraaortic	NE, NMN, CgA
4	F	<i>HIF2A</i>	36	46	R paraaortic	Negative
5	F	No mutation found	57	57	L paracaval	NMN, CgA
6	F	No mutation found	39	39	R adrenal	NMN, NE, MN, MTT, CgA
7	M	No mutation found	27	36	L adrenal	NE, NMN, DA, CgA
8	M	No mutation found	18	45	L adrenal	NE, NMN, DA, CgA
9	F	<i>PHD1</i>	25	50	R paraadrenal	NE, NMN, MN, MTT, CgA
10	M	<i>HIF2A</i>	15	17	L adrenal	NE, NMN, CgA, DA
11	F	No mutation found	30	30	R adrenal	NE, NMN, MTT, CgA
12	F	<i>HIF2A</i>	8	11	R paraaortic	NE, NMN, MN, MTT, CgA
13	F	<i>PHD2</i>	42	63	L adrenal	NE, NMN, CgA
14	M	No mutation found	16	27	L thoracic paraspinal	NE, DA, CgA

Age (d) = age at diagnosis; Age (s) = age at study; NE = norepinephrine; MTT = methoxytyramine; CgA = chromogranin A; DA = dopamine; NMN = normetanephrine; MN = metanephrine.

TABLE 2
Hematologic Characteristics and Polycythemia During NIH Evaluation

Patient no.	Sex	Phlebotomy	Hemoglobin (g/dL)	Hematocrit (%)	Erythropoietin (mIU/mL)
1	F	Every 3–6 mo	16.6 (11.2–15.7)	54.6 (34.1–44.9)	112 (2.6–18.5)
2	F	Irregular	18.6 (11.2–15.7)	63.5 (34.1–44.9)	102 (2.6–18.5)
3	F	Every 3–6 mo	11.3 (11.2–15.7)	45.1 (34.1–44.9)	231 (2.6–18.5)
4	F	Irregular	10.7 (11.2–15.7)	36.2 (34.1–44.9)	73 (2.6–18.5)
5	F	Every 3–6 mo	11.3 (11.2–15.7)	38.5 (34.1–44.9)	140 (2.6–18.5)
6	F	Every 3–6 mo	14.2 (11.2–15.7)	45.2 (34.1–44.9)	19.5 (2.6–18.5)
7	M	Every 3 wk	12.8 (13.3–17.5)	42.6 (40.1–50.1)	87.2 (2.6–18.5)
8	M	Every 2 mo	19.7 (13.3–17.5)	63.0 (40.1–50.1)	26.2 (2.6–18.5)
9	F	Every 5 wk	16.5 (11.2–15.7)	51.3 (34.1–44.9)	29.1 (2.6–18.5)
10	M	Every 6–8 wk	16.2 (13.3–17.5)	50.7 (40.1–50.1)	25.8 (2.6–18.5)
11	F	Irregular	17.9 (11.2–15.7)	51.3 (34.1–44.9)	18.3 (2.6–18.5)
12	F	Every 3–6 mo	12.4 (10.6–13.2)	40.8 (32.4–39.5)	100 (2.6–18.5)
13	F	Every 2 mo	13.4 (11.2–15.7)	44.6 (34.1–44.9)	42 (2.6–18.5)
14	M	Every 3–4 mo	13.3 (13.3–17.5)	46.3 (40.1–50.1)	106 (2.6–18.5)

Data in parentheses are normal values.

Solutions). PET images were reconstructed using an iterative algorithm provided by the manufacturer, which also uses point-spread function and time of flight. Low-dose CT studies for attenuation correction and anatomic coregistration were performed without contrast.

Analysis of Data

All imaging studies were read by different, experienced nuclear medicine physicians (PET/CT scans) or radiologists (CT and MRI scans) who were masked to all other imaging and clinical data except for the diagnosis, sex, and age of the patient.

SUV_{max} was determined, and focal areas of abnormal uptake showing a higher SUV_{max} than surrounding tissue were considered lesions. All imaging studies were performed within 31 ± 43 d of each other. For regional analysis, adrenal glands, liver, abdomen/pelvis (excluding adrenal glands and liver), lungs, mediastinum, neck, and bone were analyzed separately. Lesion-to-lesion analyses were performed, and lesion-related detection rates were compared between the different imaging modalities. If the number of lesions in a region exceeded 15, the count was truncated at 15.

As previously described and supported (13,14), a positive result on at least 2 different functional imaging modalities, or at least 1 functional imaging study and confirmation on CT/MRI, was counted as true disease. Furthermore, histologic proof was available for 18 lesions. The patients were stratified and evaluated separately between *HIF2A*, *PHD*, and unknown mutations, as well as for the entire study cohort.

Statistics

Results are given as means with 95% confidence intervals (CIs) unless stated otherwise. For statistical analysis, the McNemar test was used to compare sensitivities between the different imaging modalities. A 2-sided *P* value of less than 0.05 was considered significant.

RESULTS

¹⁸F-FDOPA, identifying 73 of 74 lesions, and ¹⁸F-FDA PET/CT, identifying 57 of 58 lesions, demonstrated lesion-based detection rates of 98.7% (95% CI, 92.7%–99.8%) and 98.3% (95% CI, 90.9%–99.7%), respectively. Fourteen patients underwent an ¹⁸F-DOPA scan, whereas only 11 underwent an ¹⁸F-FDA PET/CT scan. ¹⁸F-FDOPA and ¹⁸F-FDA PET/CT each identified significantly more lesions than ¹⁸F-FDG PET/CT (2-sided *P* < 0.01), ⁶⁸Ga-DOTATATE PET/CT (2-sided *P* < 0.01), and anatomic imaging studies with CT/MRI (2-sided *P* < 0.01), separately. The stratification of patients into 3 subgroups (*HIF2A*, *PHD*, and patients without a known mutation) did not show any significant changes in sensitivities compared with the combined patient group. Lesion-based findings comparing all functional imaging modalities as well as CT/MRI in the mentioned subgroups and in different locations are summarized in Tables 3–7.

TABLE 3
Number of Identified Lesions in ⁶⁸Ga-DOTATATE, ¹⁸F-FDG, ¹⁸F-FDOPA, ¹⁸F-FDA PET/CT, and CT/MRI, Stratified by Genetic Background and Compared with Lesions Identified by Imaging Comparator

Lesion	⁶⁸ Ga-DOTATATE	¹⁸ F-FDG	¹⁸ F-FDOPA	¹⁸ F-FDA	CT/MRI
Combined	24/68	22/52	73/74	57/58	44/74
<i>HIF2A</i>	10/20	11/26	25/26	14/15	18/26
<i>PHD</i>	1/5	3/5	5/5	3/3	2/5
Unknown mutation	13/43	8/21	43/43	40/40	24/43

TABLE 4

Detection Rate (%) and 95% CIs (%) for ⁶⁸Ga-DOTATATE, ¹⁸F-FDG, ¹⁸F-FDOPA, ¹⁸F-FDA PET/CT, and CT/MRI, Stratified by Genetic Background

Lesion	⁶⁸ Ga-DOTATATE	¹⁸ F-FDG	¹⁸ F-FDOPA	¹⁸ F-FDA	CT/MRI
Combined	35.3 (25.0–47.2)	42.3 (29.9–55.8)	98.7 (92.7–99.8)	98.3 (90.9–99.7)	60.3 (48.8–70.7)
<i>HIF2A</i>	50.0 (29.9–70.0)	42.3 (25.5–61.1)	96.1 (81.1–99.3)	93.3 (70.2–98.8)	69.2 (50.0–83.5)
<i>PHD</i>	20.0 (3.6–62.5)	60.0 (23.1–88.2)	100 (56.6–100)	100 (43.9–100)	40.0 (11.8–76.9)
Unknown mutation	30.2 (18.6–45.1)	38.1 (20.7–59.1)	100 (91.8–100)	100 (91.2–100)	55.8 (41.1–69.6)

Histopathologic proof was feasible for 18 lesions in 5 patients. Three of these histologically confirmed lesions were positive only on ¹⁸F-FDOPA PET/CT and negative on all other imaging modalities, including CT and MRI.

In 4 patients, metastatic lesions were found in retroperitoneal lymph nodes, liver, and bones. On ¹⁸F-FDOPA, 4 additional liver lesions and 3 additional abdominal lesions were seen, which were not positive on any other imaging modality or verified by histopathology, and were therefore counted as possibly false-positive. Possible false-positive results for ⁶⁸Ga-DOTATATE were found in 1 bone lesion, for ¹⁸F-FDA in 4 abdominal lesions, and for ¹⁸F-FDG in 5 abdominal lesions. Two positive lesions on ¹⁸F-FDG were confirmed as metastatic somatostatinoma in a patient with an *HIF2A* mutation. However, many other somatostatinoma metastases (confirmed by histopathology) in this patient were negative on ¹⁸F-FDG and also negative on all other imaging modalities, including anatomic, investigated in this study. Therefore, these negative somatostatinoma lesions were excluded from our evaluation.

⁶⁸Ga-DOTATATE PET/CT was falsely and completely negative in 2 patients with 5 lesions identified on at least 2 other imaging modalities. ¹⁸F-FDG PET/CT was totally negative in 1 patient with 5 similarly detected lesions.

Mean SUV_{max} for identified lesions was 33.7 ± 18.3 for ⁶⁸Ga-DOTATATE, 10.8 ± 4.6 for ¹⁸F-FDG, 40.8 ± 20.9 for ¹⁸F-FDOPA, and 23.1 ± 13.5 for ¹⁸F-FDA.

A PET imaging example comparing ⁶⁸Ga-DOTATATE, ¹⁸F-FDG, ¹⁸F-FDOPA, and ¹⁸F-FDA PET/CT in the same patient is shown in Figure 1.

DISCUSSION

We present the largest study evaluating the functional imaging signature of patients presenting with the rare PPGL–polycythemia

syndromes using 4 different PET radiopharmaceuticals, including ⁶⁸Ga-DOTATATE, ¹⁸F-FDG, ¹⁸F-FDOPA, and ¹⁸F-FDA, as well as CT and MRI.

¹⁸F-FDOPA and ¹⁸F-FDA PET/CT showed similar, significantly higher detection rates, 98.6% and 98.3%, respectively, than all other investigated imaging modalities in this study. Stratification of patients into 3 subgroups (*HIF2A*, *PHD*, and patients without a known mutation) did not show any significant differences compared with the entire study cohort.

¹⁸F-FDOPA and ¹⁸F-FDA are both specific radiopharmaceuticals. ¹⁸F-FDOPA targets the cell via the large amino acid transporter system (15), has previously shown good diagnostic results in other neuroendocrine tumors (15), and is currently recommended for head and neck PGL imaging as well as for metastatic disease in sporadic metastatic PGL (16).

¹⁸F-FDA specifically enters the cell via the norepinephrine transporter and targets the catecholamine synthesis, storage, and secretion pathways (17,18). Although ¹⁸F-FDA has shown mixed results in patients with more dedifferentiated PPGLs with underlying *SDH* subunit *B* (*SDHB*) mutations, it has shown a good diagnostic accuracy in primary as well as metastatic sporadic PPGLs (19–21). Although some of the patients in our cohort had metastatic disease, the excellent and almost equal diagnostic performance of ¹⁸F-FDOPA and ¹⁸F-FDA in all patients evaluated in this study suggests that PPGLs in patients with PPGL–polycythemia syndromes are, in general, more well-differentiated tumors in which the expression and function of large amino acid transporter and norepinephrine transporter systems is not significantly impaired. This is supported by the biochemical phenotype of these tumors (Table 1).

Although the diagnostic utility of ¹²³I-metaiodobenzylguanidine (MIBG), which was not evaluated in this study, is known to be inferior to ¹⁸F-FDA (19), the evaluation of ¹²³I-MIBG uptake

TABLE 5

Number of Identified Lesions in ⁶⁸Ga-DOTATATE, ¹⁸F-FDG, ¹⁸F-FDOPA, ¹⁸F-FDA PET/CT, and CT/MRI Compared with Lesions Identified by Imaging Comparator Based on Lesion Location

Lesion	⁶⁸ Ga-DOTATATE	¹⁸ F-FDG	¹⁸ F-FDOPA	¹⁸ F-FDA	CT/MRI
All compartments	24/68	22/52	73/74	57/58	44/74
Neck	1/1	0/1	1/1	1/1	0/1
Adrenal R	0/1	0/1	1/1	1/1	1/1
Adrenal L	1/2	0/2	2/2	1/1	2/2
Abdomen	19/46	22/47	52/52	37/37	33/52
Liver	3/12	0/1	11/12	11/12	5/12
Bone	0/6	0/0	6/6	6/6	3/6

TABLE 6

Detection Rate (%) and 95% CIs (%) for ⁶⁸Ga-DOTATATE, ¹⁸F-FDG, ¹⁸F-FDOPA, ¹⁸F-FDA PET/CT, and CT/MRI Based on Lesion Location

Detection rate	⁶⁸ Ga-DOTATATE	¹⁸ F-FDG	¹⁸ F-FDOPA	¹⁸ F-FDA	CT/MRI
All compartments	35.3 (25.0–47.2)	42.3 (29.9–55.8)	98.7 (92.7–99.8)	98.3 (90.9–99.7)	60.3 (48.8–70.7)
Neck	100 (20.7–100)	0.0 (0.0–79.4)	100 (20.7–100)	100 (20.7–100)	0.0 (0.0–79.4)
Adrenal R	0.0 (0.0–79.4)	0.0 (0.0–79.4)	100 (20.7–100)	100 (20.7–100)	0.0 (0.0–79.4)
Adrenal L	50 (9.5–90.6)	0.0 (0.0–65.6)	100 (34.2–100)	100 (34.2–100)	100 (34.2–100)
Abdomen	41.3 (28.3–55.6)	46.8 (33.3–60.8)	100 (93.1–100)	100 (90.6–100)	63.5 (49.9–75.2)
Liver	25.0 (8.9–53.2)	0.0 (0.0–79.4)	91.7 (64.6–98.5)	91.7 (64.6–98.5)	41.7 (19.3–68.1)
Bone	0.0 (0.0–39.1)	—	100 (61.0–100)	100 (61.0–100)	50.0 (18.7–81.2)

might be of importance in these patients because ¹²³I-MIBG and ¹⁸F-FDA enter the cell via the same transporter-system (21) and ¹²³I-MIBG uptake identifies patients who are potentially eligible for ¹³¹I-MIBG treatment. Considering the limited availability of ¹⁸F-FDOPA and ¹⁸F-FDA, and the limited diagnostic value of ¹⁸F-FDG and ⁶⁸Ga-DOTATATE in this study, ¹²³I-MIBG could be an appropriate diagnostic imaging modality for this group of patients. However, the utility of ¹²³I-MIBG needs further evaluation.

¹⁸F-FDG is currently the radiopharmaceutical of choice in metastatic PPGL (22–24) and has good accuracy, especially in patients with more dedifferentiated tumors and underlying *SDHB* mutations (20,25). These tumors show upregulated expression of glucose transporters as well as an upregulation of hexokinase, which explains the high ¹⁸F-FDG uptake in tumors with *SDH* subunit A–D (collectively *SDHx*) deficiency (26,27). These tumors belong to the cluster 1 pseudohypoxic tumors and are believed to be associated with HIF stabilization (28). Furthermore, an upregulation of glucose transporters was shown in *HIF2A* and *PHD* mutation-related tumors (11,28). However, despite these similarities to *SDHx*-related tumors, the tumors in our patient cohort showed a low detection rate for ¹⁸F-FDG PET/CT, which could possibly be explained by a lack of hexokinase upregulation, which has been shown in *HIF2A*-mutated tumors (28).

⁶⁸Ga-DOTATATE PET/CT was recently introduced into PPGL imaging and has shown excellent results in the patient groups evaluated thus far, which mainly include those with sporadic and *SDHB*-related metastatic PPGL as well as head and neck PGLs (13,29–34).

If metastatic tumors are positive on ⁶⁸Ga-DOTATATE, patients may be eligible for peptide receptor radionuclide therapy. In studies performed at our institution, ⁶⁸Ga-DOTATATE was superior to ¹⁸F-FDOPA, ¹⁸F-FDA, and ¹⁸F-FDG in most patients studied so far (13,30). Therefore, the low lesion detection rate in the PPGL–polycythemia patient cohort was surprising. In fact, ⁶⁸Ga-DOTATATE had the lowest lesion detection rate among all of the imaging procedures, identifying only 35.8% of all lesions, indicating that most of the patients in this patient cohort would be poor candidates for peptide receptor radionuclide therapy, because only a minority of lesions showed significant ⁶⁸Ga-DOTATATE uptake.

Future studies need to investigate whether the poor performance of ⁶⁸Ga-DOTATATE in this patient cohort is due to a lack of somatostatin receptor (SSR) expression, inactivation of SSR, or overexpression of SSR of other subtypes that could potentially be visualized with ⁶⁸Ga-DOTATOC or ⁶⁸Ga-DOTANOC, because these radiopharmaceuticals show affinity for SSR3 and SSR5, whereas ⁶⁸Ga-DOTATATE shows selective affinity for SSR2 (35).

False-positive lesions were found with every radiopharmaceutical. The fact that some lesions were identified only by ¹⁸F-FDOPA, and were confirmed by histopathology, suggests that some of the lesions counted as false-positive could have actually been true-positive disease. Two positive lesions on ¹⁸F-FDG were found in a patient who also had confirmed metastatic somatostatinoma related to her *HIF2A* mutation. Therefore, it may be that the ¹⁸F-FDG–positive lesions in this patient are

TABLE 7

Number of Identified Lesions in ⁶⁸Ga-DOTATATE, ¹⁸F-FDG, ¹⁸F-FDOPA, ¹⁸F-FDA PET/CT, and CT/MRI Compared with Lesions Identified by Imaging Comparator Based on Lesion Location for Patients Who Underwent Imaging with All PET Radiopharmaceuticals

Lesions	⁶⁸ Ga-DOTATATE	¹⁸ F-FDG	¹⁸ F-FDOPA	¹⁸ F-FDA	CT/MRI
All compartments	20/52	13/52	51/52	51/52	31/52
Neck	1/1	0/1	1/1	1/1	0/1
Adrenal R	0/0	0/0	0/0	0/0	0/0
Adrenal L	1/1	0/1	1/1	1/1	1/1
Abdomen	15/32	13/32	32/32	32/32	22/32
Liver	3/12	0/12	11/12	11/12	5/12
Bone	0/6	0/6	6/6	6/6	3/6

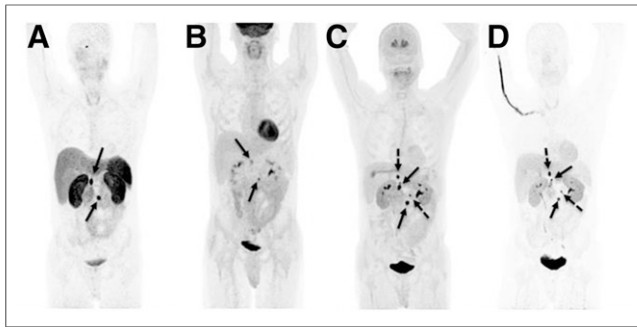


FIGURE 1. A 44-y-old male with multiple abdominal paragangliomas was first diagnosed with a left adrenal pheochromocytoma at age 18. No mutation was found. He required phlebotomies since early childhood due to polycythemia. ^{68}Ga -DOTATATE PET (A) demonstrated 2 retroperitoneal lesions, also faintly seen on ^{18}F -FDG PET (B) (solid arrows). ^{18}F -FDOPA PET (C) and ^{18}F -FDA PET (D) similarly showed additional retroperitoneal lesions (dotted arrows). Images are shown as maximum-intensity projections.

related to somatostatinoma. On the basis of the limited experience in this single patient, confirmation of her metastatic somatostatinoma also suggests that ^{68}Ga -DOTATATE, ^{18}F -FDOPA, and ^{18}F -FDA are unlikely to detect somatostatinoma-related lesions.

Our study has several limitations. Although this is the largest cohort with PPGL–polycythemia patients evaluated to date, the sample size is still small. However, this is not surprising, because this is a rare syndromic presentation. Only Därr et al. have already investigated the clinical and imaging features in a group consisting of 7 *HIF2A* patients, also showing good lesion detection rates with ^{18}F -FDOPA PET/CT (36). Although Därr et al. focused solely on *HIF2A*-related PPGL and polycythemia, our study investigated patients with *HIF2A*-, *PHD1*-, and *PHD2*-related mutations, as well as patients with identical clinical presentations, but no known mutations. Furthermore, histologic proof was neither feasible nor ethical for many lesions, although our imaging comparator might have given a good approximation of truth.

CONCLUSION

The specific, well-established radiopharmaceuticals ^{18}F -FDOPA and ^{18}F -FDA showed excellent and equal diagnostic performance in lesion detection in PPGL–polycythemia patients, detecting significantly more lesions than ^{18}F -FDG, ^{68}Ga -DOTATATE, and anatomic imaging with CT/MRI, irrespective of the underlying mutation status. Therefore, ^{18}F -FDOPA and ^{18}F -FDA appear to be the preferred radiopharmaceuticals for evaluation of this rare group of patients. However, ^{18}F -FDOPA and especially ^{18}F -FDA are of limited availability. Because ^{18}F -FDA and $^{123/131}\text{I}$ -MIBG use the same transporter system, these patients may be excellent candidates for $^{123/131}\text{I}$ -MIBG imaging and treatment. This needs to be evaluated in future studies.

DISCLOSURE

This work was supported, in part, by the Intramural Research Program of the NIH, Eunice Kennedy Shriver NICHD. No other potential conflict of interest relevant to this article was reported.

ACKNOWLEDGMENTS

We thank the patients, their families, and their referring physicians, as well as the technologists in the NIH PET Department.

REFERENCES

- DeLellis RA. *Pathology and Genetics of Tumours of Endocrine Organs*. Lyon, France: IARC Press; 2004.
- Timmers HJ, Kozupa A, Eisenhofer G, et al. Clinical presentations, biochemical phenotypes, and genotype-phenotype correlations in patients with succinate dehydrogenase subunit B-associated pheochromocytomas and paragangliomas. *J Clin Endocrinol Metab*. 2007;92:779–786.
- Brouwers FM, Eisenhofer G, Tao JJ, et al. High frequency of SDHB germline mutations in patients with malignant catecholamine-producing paragangliomas: implications for genetic testing. *J Clin Endocrinol Metab*. 2006;91:4505–4509.
- Benn DE, Robinson BG, Clifton-Bligh RJ. 15 years of paraganglioma: clinical manifestations of paraganglioma syndromes types 1-5. *Endocr Relat Cancer*. 2015;22:T91–T103.
- Amar L, Bertherat J, Baudin E, et al. Genetic testing in pheochromocytoma or functional paraganglioma. *J Clin Oncol*. 2005;23:8812–8818.
- Castro-Vega LJ, Buffet A, De Cubas AA, et al. Germline mutations in FH confer predisposition to malignant pheochromocytomas and paragangliomas. *Hum Mol Genet*. 2014;23:2440–2446.
- Burnichon N, Cascon A, Schiavi F, et al. MAX mutations cause hereditary and sporadic pheochromocytoma and paraganglioma. *Clin Cancer Res*. 2012;18:2828–2837.
- Pacak K, Jochmanova I, Prodanov T, et al. New syndrome of paraganglioma and somatostatinoma associated with polycythemia. *J Clin Oncol*. 2013;31:1690–1698.
- Zhuang Z, Yang C, Lorenzo F, et al. Somatic HIF2A gain-of-function mutations in paraganglioma with polycythemia. *N Engl J Med*. 2012;367:922–930.
- Ladroue C, Carcenac R, Leporrier M, et al. PHD2 mutation and congenital erythrocytosis with paraganglioma. *N Engl J Med*. 2008;359:2685–2692.
- Yang C, Zhuang Z, Flidner SM, et al. Germ-line PHD1 and PHD2 mutations detected in patients with pheochromocytoma/paraganglioma-polycythemia. *J Mol Med*. 2015;93:93–104.
- Franke K, Gassmann M, Wielockx B. Erythrocytosis: the HIF pathway in control. *Blood*. 2013;122:1122–1128.
- Janssen I, Blanchet EM, Adams K, et al. Superiority of [^{68}Ga]-DOTATATE PET/CT to other functional imaging modalities in the localization of SDHB-associated metastatic pheochromocytoma and paraganglioma. *Clin Cancer Res*. 2015;21:3888–3895.
- Hofman MS, Hicks RJ. Moving Beyond “Lumpology”: PET/CT imaging of pheochromocytoma and paraganglioma. *Clin Cancer Res*. 2015;21:3815–3817.
- Santhanam P, Taieb D. Role of ^{18}F -FDOPA PET/CT imaging in endocrinology. *Clin Endocrinol (Oxf)*. 2014;81:789–798.
- Taieb D, Timmers HJ, Hindie E, et al. EANM 2012 guidelines for radionuclide imaging of pheochromocytoma and paraganglioma. *Eur J Nucl Med Mol Imaging*. 2012;39:1977–1995.
- Pacak K, Eisenhofer G, Carrasquillo JA, Chen CC, Li ST, Goldstein DS. 6-[^{18}F]fluorodopamine positron emission tomographic (PET) scanning for diagnostic localization of pheochromocytoma. *Hypertension*. 2001;38:6–8.
- Eisenhofer G, Hovey-Sion D, Kopin JJ, et al. Neuronal uptake and metabolism of 2- and 6-fluorodopamine: false neurotransmitters for positron emission tomographic imaging of sympathetically innervated tissues. *J Pharmacol Exp Ther*. 1989;248:419–427.
- Timmers HJ, Eisenhofer G, Carrasquillo JA, et al. Use of 6-[^{18}F]-fluorodopamine positron emission tomography (PET) as first-line investigation for the diagnosis and localization of non-metastatic and metastatic pheochromocytoma (PHEO). *Clin Endocrinol (Oxf)*. 2009;71:11–17.
- Timmers HJ, Kozupa A, Chen CC, et al. Superiority of fluorodeoxyglucose positron emission tomography to other functional imaging techniques in the evaluation of metastatic SDHB-associated pheochromocytoma and paraganglioma. *J Clin Oncol*. 2007;25:2262–2269.
- Timmers HJ, Chen CC, Carrasquillo JA, et al. Comparison of ^{18}F -fluoro-L-DOPA, ^{18}F -fluoro-deoxyglucose, and ^{18}F -fluorodopamine PET and ^{123}I -MIBG scintigraphy in the localization of pheochromocytoma and paraganglioma. *J Clin Endocrinol Metab*. 2009;94:4757–4767.

22. Lenders JW, Duh QY, Eisenhofer G, et al. Pheochromocytoma and paraganglioma: an endocrine society clinical practice guideline. *J Clin Endocrinol Metab.* 2014;99:1915–1942.
23. Mann GN, Link JM, Pham P, et al. [¹¹C]metahydroxyephedrine and [¹⁸F]fluorodeoxyglucose positron emission tomography improve clinical decision making in suspected pheochromocytoma. *Ann Surg Oncol.* 2006;13:187–197.
24. Shulkin BL, Thompson NW, Shapiro B, Francis IR, Sisson JC. Pheochromocytomas: imaging with 2-[fluorine-18]fluoro-2-deoxy-D-glucose PET. *Radiology.* 1999;212:35–41.
25. Timmers HJ, Chen CC, Carrasquillo JA, et al. Staging and functional characterization of pheochromocytoma and paraganglioma by ¹⁸F-fluorodeoxyglucose (¹⁸F-FDG) positron emission tomography. *J Natl Cancer Inst.* 2012;104:700–708.
26. Favier J, Briere JJ, Burnichon N, et al. The Warburg effect is genetically determined in inherited pheochromocytomas. *PLoS One.* 2009;4:e7094.
27. Mathupala SP, Ko YH, Pedersen PL. Hexokinase-2 bound to mitochondria: cancer's stygian link to the "Warburg Effect" and a pivotal target for effective therapy. *Semin Cancer Biol.* 2009;19:17–24.
28. Jochmanová I, Yang C, Zhuang Z, Pacak K. Hypoxia-inducible factor signaling in pheochromocytoma: turning the rudder in the right direction. *J Natl Cancer Inst.* 2013;105:1270–1283.
29. Tan TH, Hussein Z, Saad FF, Shuaib IL. Diagnostic performance of ⁶⁸Ga-DOTA-TATE PET/CT, ¹⁸F-FDG PET/CT and ¹³¹I-MIBG scintigraphy in mapping metastatic pheochromocytoma and paraganglioma. *Nucl Med Mol Imaging.* 2015;49:143–151.
30. Janssen I, Chen CC, Taieb D, et al. ⁶⁸Ga-DOTATATE PET/CT in the localization of head and neck paragangliomas compared to other functional imaging modalities and CT/MRI. *J Nucl Med.* 2016;57:186–191.
31. Naji M, Zhao C, Welsh SJ, et al. ⁶⁸Ga-DOTA-TATE PET vs. ¹²³I-MIBG in identifying malignant neural crest tumours. *Mol Imaging Biol.* 2011;13:769–775.
32. Win Z, Al-Nahhas A, Towey D, et al. ⁶⁸Ga-DOTATATE PET in neuroectodermal tumours: first experience. *Nucl Med Commun.* 2007;28:359–363.
33. Sharma P, Thakar A, Suman KCS, et al. ⁶⁸Ga-DOTANOC PET/CT for baseline evaluation of patients with head and neck paraganglioma. *J Nucl Med.* 2013;54:841–847.
34. Naswa N, Sharma P, Nazar AH, et al. Prospective evaluation of ⁶⁸Ga-DOTA-NOC PET-CT in phaeochromocytoma and paraganglioma: preliminary results from a single centre study. *Eur Radiol.* 2012;22:710–719.
35. Reubi JC, Schar JC, Waser B, et al. Affinity profiles for human somatostatin receptor subtypes SST1-SST5 of somatostatin radiotracers selected for scintigraphic and radiotherapeutic use. *Eur J Nucl Med.* 2000;27:273–282.
36. Därr R, Nambuba J, Del Rivero J, et al. Novel insights into the polycythemia-paraganglioma-somatostatinoma syndrome. *Endocr Relat Cancer.* 2016;23: 899–908.